Electronic Journal of Structural Engineering

Original Article

Cite this: DOI:10.56748/ejse.26876

Received Date: 4 September 2025
Accepted Date:28 November 2025

1443-9255
https://ejsei.com/ejse

Investigation of the Residual Structural Performance of Hollow Section Stub Columns Under Eccentric Axial Compression Following Fire Exposure

Xiangyun Wan [a*], Yiju Tang [a]

[a] Henan University of Urban Construction; Pingdingshan, Henan, 467036, China
*Corresponding author: xywan51@huuc.edu.cn

Abstract

The study looks at how much load the hollow section stub columns can bear after they are subjected to non-central axially compressed eccentricity and have been exposed to very high temperatures. This is done to foster the grasp of the fire behavior of such structures. Some finite element (FE) schemes representing the experimental configurations were created and tested against the test data to simulate the mechanical behavior of the ultra-high-strength steel (UHSS) columns with different geometrical and loading conditions. The variables under study included cross-sectional shape (round and square), cross-sectional area, thickness of the wall, and eccentricity in X and Y directions. The results showed that circular columns had more load capacity at the point of failure than square columns, particularly at elevated temperatures. In addition, increasing the cross-sectional dimensions and wall thickness was beneficial for the ultimate load capacity and fire resistance; however, increased eccentricity led to significant decreases in ultimate strength and caused asymmetric deformation accompanied by complicated buckling modes. The calibrated schemes reproduced the experimental behaviors and provided insights into the impact of geometrical factors on thermal degradation.

Keywords

Post-fire behavior, Hollow section stub columns, Eccentric loading, UHSS, FE analysis

1. Introduction

The structural stability and dependability of steel columns regarding fire threats have long been a significant concern in structural engineering (Golzadeh Ebrahimi, 2025; Qureshi et al., 2022). Hollow structural sections (HSS) are a specific category of steel members characterized by their superior strength-to-weight ratio, visually appealing geometric forms, and resistance to torsion (Khalaf et al., 2022). However, it is generally acknowledged that those structures that rely on a fire load can lose their fire resistance. Despite that, columns are expected to be able to carry partially or even fully the service load after the fire incident, thus ensuring long-term support of the materials transportation in the infrastructures that are necessary for the fixes and restoration (Dadvand, 2025; Zhong et al., 2022). Consequently, it is of primary importance to understand the changes in the behavior of steel columns during the recovery process after a fire, in particular, the short columns, which are distinguished by compactness and a high local strength factor. Steel columns' post-fire performance is vital for the identification of safety levels during structures' assessment after an incident and the decision-making process. In a fire scenario, which is subject to extensive research, is mainly considered full-length columns, beams, and beam-columns, while the majority of the studies are limited to these. Besides, the residual performance of stub columns, especially those eccentrically loaded, has been overlooked; thus, the research findings in that area are very limited. This, in turn, would most likely lead to a better understanding of the flaws and misalignments that are usually found in practice. The gaps that remain in the research are the steel mechanical properties post-fire and the effect of geometrical factors, including cross-section type, thickness of the wall, and load eccentricity, on the behavior of the stub columns. Investigation of these variables is indispensable for ensuring accurate structure schemes and secure design principles for systems subjected to fire.

1.1 Literature Review

Zuo et al. (Zuo et al., 2024) and Zhong et al. (Zhong, Sun, et al., 2021) reviewed the post-fire performance of cold-form elliptical and high-strength tubular steel stub columns, revealing that traditional design equations, including DSM and equivalent diameter methods, underestimated residual strength, whereas modified DSM and design interaction curves yielded more accurate predictions. He et al. (He et al., 2021) and Xing et al. (Xing et al., 2024) reviewed fire-exposed austenitic stainless steel circular hollow section (CHS) stub columns under combined loads and confirmed that the Continuous Strength Method (CSM) yielded more dependable results than conventional code provisions. Numerous studies have examined steel-reinforced concrete (SRC) columns exposed to eccentric compression and corresponding design fire scenarios. Xiao-yong (Jinxue et al., 2010) examined the behavior of SRC columns under ISO-834 standard fire conditions and subsequent cooling, highlighting the significant impact of loading during heating and the variations in failure modes observed at ambient temperature compared to post-fire conditions. Al-Thairy and Al-Naqeeb (Al-Thairy et al., 2023) conducted a numerical simulation of eccentrically loaded lightweight reinforced concrete (LWRC) columns subjected to elevated temperatures, demonstrating that ultimate capacity is influenced by the duration and distribution of temperatures, and the thickness of the concrete cover. Hodovanets and Kvočák (Hodovanets et al., 2024) and Grajçevci et al. (Grajçevci et al., 2024) investigated cold-formed rectangular hollow section (RHS) and CHS columns under eccentric loading and geometric flaws, concluding that the likelihood of instability escalated with eccentric loading. Chen et al. (Chen et al., 2020) examined CHS stub columns constructed from high-strength steels (Q460, Q690, Q960) and analyzed the inadequacies of the existing limits and design equations outlined in analytical codes, therefore surpassing these constraints by proposing enhanced slenderness limits and design equations. Liu et al. (J. Liu et al., 2023) examined irregular hexagonal hollow sections subjected to combined loading, indicating that current standards like EC3 and AISC are excessively cautious as they do not account for strain hardening, which can be alleviated with CSM. Zhang et al. (Zhang et al., 2025; Zhang, Su, et al., 2024c, 2024a; Zhang, Yang, et al., 2024a) investigated various testing methods and FE modeling of S890 and S960 UHSS CHS stub columns and beam-columns subjected to fire exposure. Their findings validated that American standards surpass European and Australian methods for evaluating structural steel, especially for slender members, and introduced new retention factor curves along with an alternative interaction design methodology. Xing et al. (Xing et al., 2023) investigated QN1803 stainless steel stub columns and proposed a novel design formulation that surpasses the EN 1993-1-2 specifications. Zhao et al. (Zhao et al., 2024) reviewed the productivity of recycled aggregate CFST stub columns following exposure to fire in alternative and sustainable buildings. Their findings indicated that an increased proportion of recycled material led to diminished rigidity and bearing capability. Liu et al. (J.-Z. Liu et al., 2024) investigated Q690 press-braked EHS stub columns, proposing new slenderness limitations and recommending the application of DSM and CSM due to the distinct buckling behavior compared to hot-rolled and cold-formed columns. Fang et al. (Fang et al., 2019) and Chen et al. (Chen et al., 2021) have reviewed octagonal steel hollow sections and have suggested updated classification and design methodologies that are not addressed by existing guidelines. Meng and

Gardner (Meng et al., 2021) contributed by evaluating the buckling behavior of high-strength CHS columns and proposed enhancements to Eurocode 3 (EC3) based on their findings, which incorporated additional effects of yield strength. Zhou et al. (H. Zhou et al., 2019) examined the thermal degradation of mechanical traits in HSSs and proposed predictive equations for post-fire behavior, primarily based on material thickness, attained temperature, and the application of cooled or uncooled methods. Ultimately, Sun et al. (Y. Sun et al., 2024) studied the behaviors of stub columns constructed from aluminum angle sections. They confirmed that torsional buckling was the predominant failure mode and that the Eurocode and Australian/New Zealand design guidelines inadequately address the failure modes of such sections. Recent studies have further advanced understanding of post-fire behavior in UHSS members. Su et al. (Su et al., 2021) examined S690 welded I-section stub columns, demonstrating that ambient-temperature design provisions are effective under post-fire conditions. Sun and Su (Z. Sun et al., 2025) examined Q960 UHSS welded I-sections under major-axis mixed loading and reported significant stiffness and strength degradation after thermal exposure, highlighting the influence of redistribution of residual stress. Uszball et al. (Uszball et al., 2024) evaluated the post-fire mechanical properties of high- and UHSSs, showing that yield and tensile strengths can retain over 70 % of their ambient values even after exposure to 700–800 °C. Azhari et al. (Azhari et al., 2017) examined cold-formed UHSS tubular stub columns and noted intricate transitions from local to global buckling following cooling. In contrast, Hu and Li (Hu et al., 2022) conducted a numerical analysis of the post-fire resistance of high-strength circular concrete-filled steel tube (CFST) stub columns, highlighting the positive impact of confinement on the retention of axial capacity. These studies collectively indicate that although the post-fire response of UHSS members has been increasingly examined, most existing works treat geometric and loading parameters independently. The interplay of cross-sectional geometry, wall thickness, and biaxial eccentricity is inadequately quantified, representing a research gap that this study directly addresses.

1.2 Research Gap

Much research has been conducted on the post-fire behavior of hollow section stub columns; however, these studies predominantly focus on standard cross-sections and conventional loading situations. The majority of studies have focused solely on certain facets of the issue, including geometry or eccentric loading, while isolating variables related to cross-sectional shape and eccentricity. The influence of varying cross-section shape, size, wall thickness, and combined eccentricity in both X and Y directions on post-fire performance has not been evaluated. No integration of these themes has been conducted to comprehend real-world structural performance in post-fire scenarios.

1.3 Novelty

This research provides a thorough and quantitative analysis of the combined influences of cross-sectional geometry, wall thickness, and biaxial eccentricity on the post-fire residual performance of UHSS hollow section stub columns. This research systematically elucidates the interactive influence of these parameters on residual strength, deformation behavior, and the evolution of complex buckling modes under combined thermal and eccentric loading conditions, in contrast to prior works that examined them in isolation.

2. Numerical Investigation

2.1 General

Numerical modeling to support the previously indicated testing program was performed utilizing the FE Method (FEM) with ABAQUS (Systemes, 2021). Finite-element schemes were initially created based on the previously mentioned experimental results, detailed in (Zhang, Su, et al., 2024b; Zhang, Yang, et al., 2024a), and subsequently expanded to perform additional parametric experiments, thus producing extensive numerical data across diverse cross-sectional geometries and load magnitudes.

2.2 FE model Development

Element type and mesh size

The S4R shell element in ABAQUS (Systemes, 2021) was selected because it was previously used to successfully model high-strength steel hollow sections (Li et al., 2019; Meng et al., 2020b, 2020a; Wang et al., 2017; Zhong, Tan, et al., 2021) and is an efficient way to model in ABAQUS, as a 4-node, reduced-integration, general-purpose shell element. An exploration was executed to review the effect of mesh size, and because of the need for balance between computational time and accuracy of the scheme, a mesh element size of 10 mm was deployed (Figure 1a).

Material modeling

The FEMs were constructed using S890 UHSS, necessitating the representative measurement of cross-sectional geometries. The Young's modulus $E = 192.344$ MPa was derived from experimental assessments (Zhang, Yang, et al., 2024a), and Poisson's ratio was assumed to be $\nu = 0.3$. Fig. 2 illustrates the experimentally obtained engineering stress–strain curve for S890 UHSS coupons subjected to 800 °C. The data were utilized to derive the true stress–strain links adopted in the FEM according to the following equations (Eqs. 1 and 2):

$$\sigma_{true=}\sigma_{eng}\left(1+\varepsilon_{eng}\right) \quad (1)$$

$$\varepsilon_{true} = ln\left(1+\varepsilon_{eng}\right) - \frac{\sigma_{true}}{E} \quad (2)$$

Note that σ_{eng} displays engineering stress and ε_{eng} indicates engineering strain.

Boundary conditions and loading

Two reference points (RPs) were created with pin-ended boundary conditions. RPs were kinematically coupled to the end surfaces of the stub column model. All degrees of freedom were constrained except for translation along the axis at the top RP and rotation about the axis at both RPs (Figure 1a). The initial eccentricity from the centroid, which simulates loading scenarios with eccentricity, is shown in Figure 1b.

2.3 Initial Geometric Imperfections and Residual Stresses

All schemes incorporated primary local geometric flaws derived from the lowest elastic buckling mode. To prevent under- or over-triggering of local wrinkling, the sensitivity to imperfection amplitude (t/20, t/100, t/200) was evaluated. Ultimate load capacity predictions demonstrated insensitivity to amplitude within a limited range, leading to the retention of t/100 for consistency. FE deformed shapes are presented at post-peak stages; the default contour scaling may visually exaggerate local wrinkles (t is the wall thickness of the scheme). Residual stresses were excluded from the analysis, as previous studies have shown that their influence on hot-rolled steel hollow sections is generally negligible compared to the yield strength resulting from homogeneous cooling processes. Specifically, residual stresses in such sections are relatively low and have minimal impact on the overall load–load-displacement behavior and ultimate capacity in FE simulations (Jandera et al., 2008; Ma et al., 2015; Mehari et al., 2022).

2.4 Solution Methodology

All simulations were conducted using the Static General analysis phase in ABAQUS, using geometric and material nonlinearities to accurately describe the nonlinear post-buckling and failure behavior of stub columns subjected to eccentric stress circumstances.

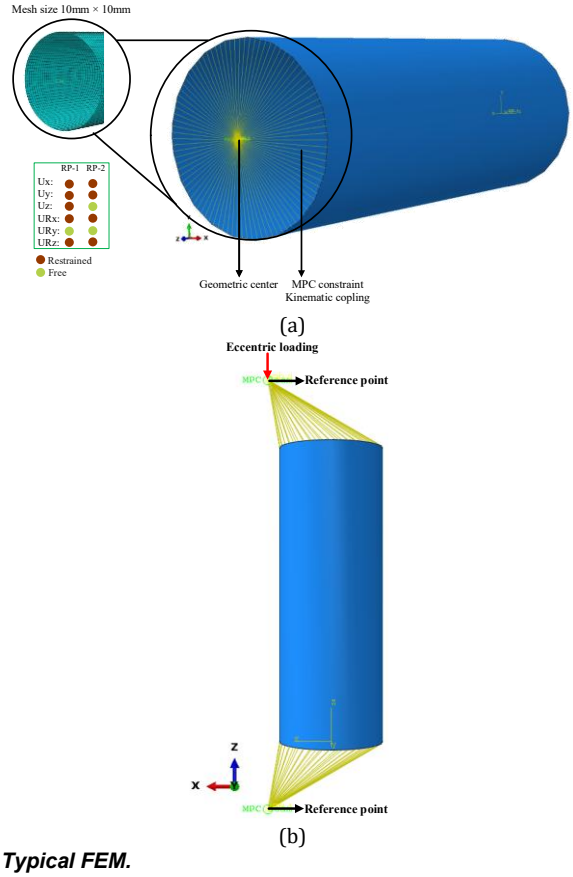

Fig. 1 Typical FEM.

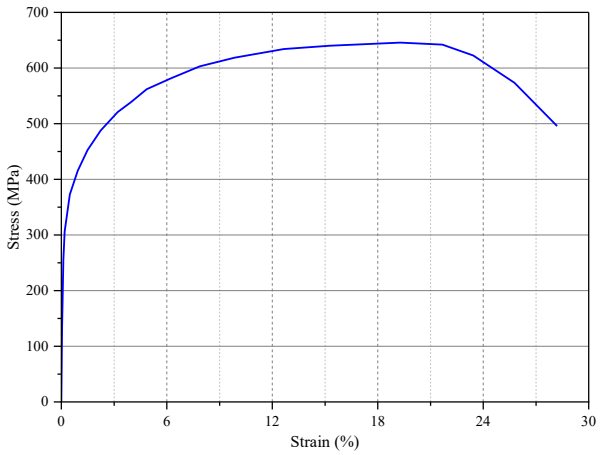

Fig. 2 Measured engineering stress–strain curves of S890 UHSS coupons after heating to 800 °C post-fire temperature (Zhang, Yang, et al., 2024b).

2.5 FE Model Verification

FE model validation for CHS column after heating

FEMs were corroborated with prior experimental findings (Zhang, Su, et al., 2024b; Zhang, Yang, et al., 2024a) for S890 UHSS hot-rolled CHS beam-columns regarding failure mechanisms, ultimate loads, and load-deflection curves. Two distinct combinations of imperfection magnitudes were employed to compare FE ultimate loads $N_{u,FE}$, with experimental findings $N_{u,test}$, revealing that $N_{u,FE}$ accurately predicted the experimental outcomes solely when utilizing the imperfection magnitude of t/100. The FEMs created were accurately calibrated to the failure modes and load-mid-height lateral deflection curves for the standard specimens of CHS-T800-E1.25 and CBC-T800-E46.3, as seen in Figure 3. The constructed FEMs precisely anticipate the empirical outcomes of the S890 UHSS CHS beam-column specimens post high-temperature exposure, and these schemes are employed for subsequent parametric analyses.

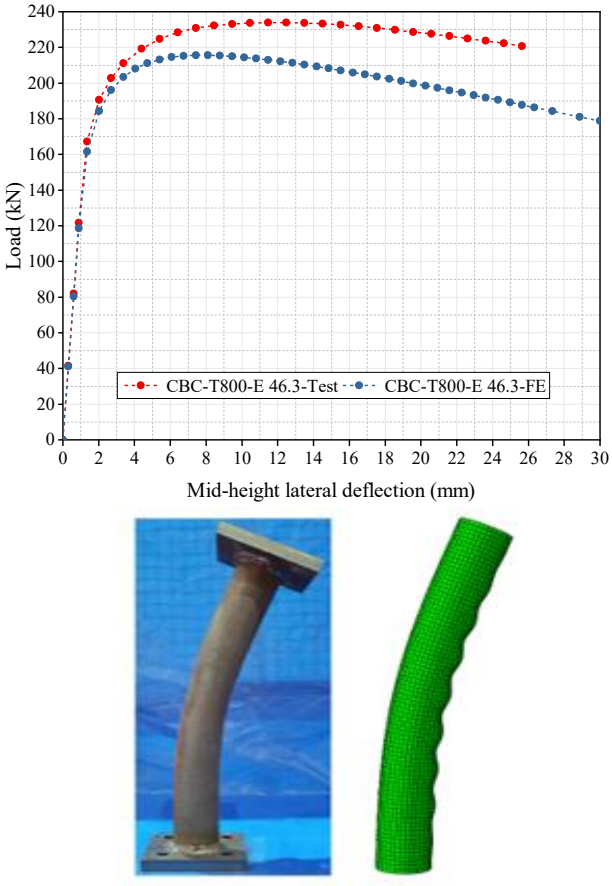

(a) CBC-T800-E46.3 (Zhang, Yang, et al., 2024a)

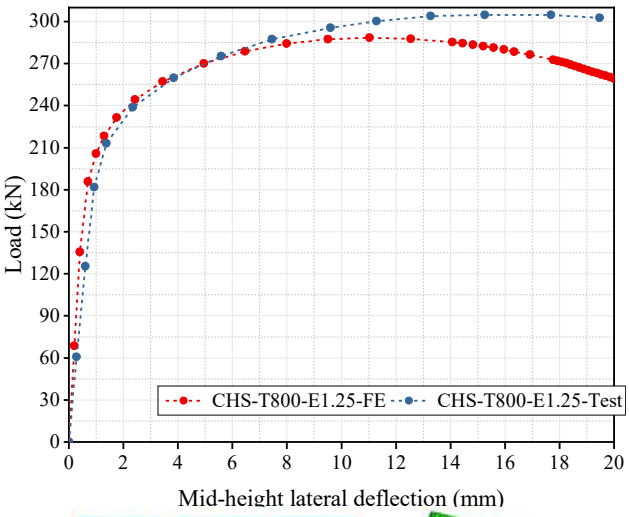

(b) CHS-T800-E1.25 (Zhang, Su, et al., 2024b)

Fig. 3 Juxtaposition of test and FE load-mid-height lateral deflection curves and failure mechanisms.

FE model validation for rectangular hollow-section column

In addition to circular hollow-section verification, the finite-element modeling approach was further validated using the R 50 × 30 × 2.5-550 rectangular hollow-section (RHS) stub column tested by Zhou et al. (F. Zhou et al., 2022). This specimen was chosen due to its geometry and slenderness ratio, which closely align with those utilized in the current numerical study. The material behavior of this model was established using the attained stress–strain curves for the flat and corner sections of the cross-section (refer to Figure 4), which were digitized from the original experimental data presented by Zhou et al. (F. Zhou et al., 2022). Distinct constitutive curves were designated for the flat and corner areas to account for the influence of cold work strengthening in the corner areas. Figure 5 illustrates that the FE projected load–shortening curve closely aligns with the empirical result, yielding a ratio of $P_{FE}/P_{exp} = 1.01$. FEM effectively replicates the initial stiffness and post-yield softening behavior, indicating that the chosen constitutive model and boundary conditions are appropriate for rectangular and square tubular sections. This validation confirms the reliability of the simulation procedure employed for all subsequent parametric analyses.

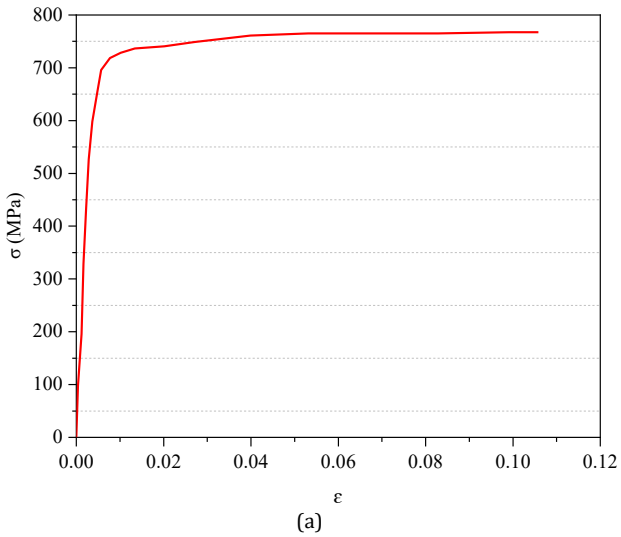

(a)

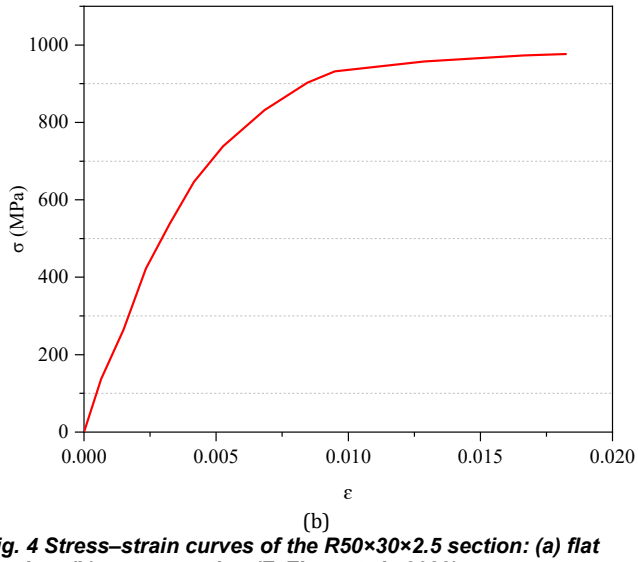

Fig. 4 Stress–strain curves of the R50×30×2.5 section: (a) flat portion, (b) corner portion (F. Zhou et al., 2022).

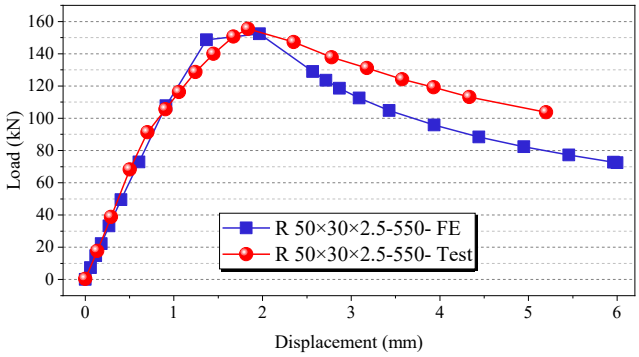

Fig. 5 Juxtaposition of empirical and numerical load–load-displacement curves (F. Zhou et al., 2022).

3. Parametric Study

The numerical results obtained from the validated FEMs are refined via a parametric analysis to determine further numerical outcomes relevant to eccentrically loaded stub columns made from UHSS Q960 (Shi et al., 2024) structural steel hollow sections following exposure to ambient and elevated temperatures (20, 600, 700, 800, and 900 degrees Celsius). The parametric study discusses the assumptions, methods, and operations discussed in detail in Part 2. Two different geometric cross-sections, i.e., circle and square, were tested. The cross-sectional variables included d and t. Here, d is the magnitude of the square and the diameter of the circle, while t is the thickness of the wall. The analyses were carried out with the local defect of the initial magnitude set at t/100. The material properties at room temperature, as well as those after exposure to high temperatures, were attained from post-fire coupon testing (Shi et al., 2024) and later used in FEMs. The first loading eccentricities were deliberately selected as d, d/2, and d/4, thus resulting in a very large number of loading combinations. 198 FE data points were produced during parametric analyses with the use of material properties at ambient temperature and after exposure to extreme temperatures. The main geometric dimensions of the stub column FEMs are displayed in Fig. 6 and Table 1. Fig. 7 displays the numerical schemes nomenclature that the parametric study involved the parameters highlighted.

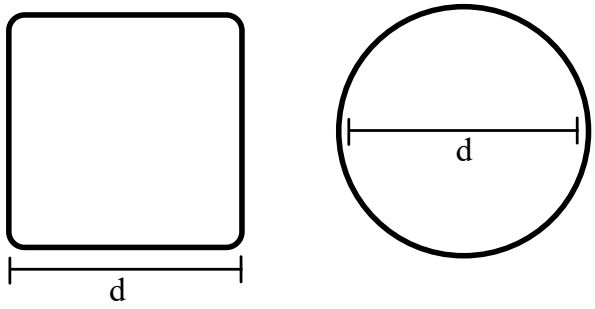

Fig. 6 Stub column cross sections.

Table 1. Geometric dimensions of stub columns deployed in the parametric exploration.

Cross-sectional shape	d (mm)	Wall thickness (mm)	Column length (mm)
Circle	150, 300	2, 4, 6	400
Square	150, 300	2, 4, 6	400

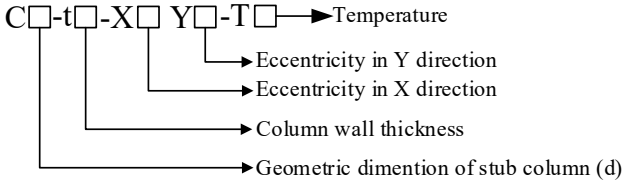

Fig. 7 Nomenclature of the numerical schemes.

4. Structural Analysis Results

This exploration reviews the axial load capacity, axial shortening, and ultimate load capabilities of several types of stub columns. The axial load curves for the stub columns are depicted in Figures 8 and 9.

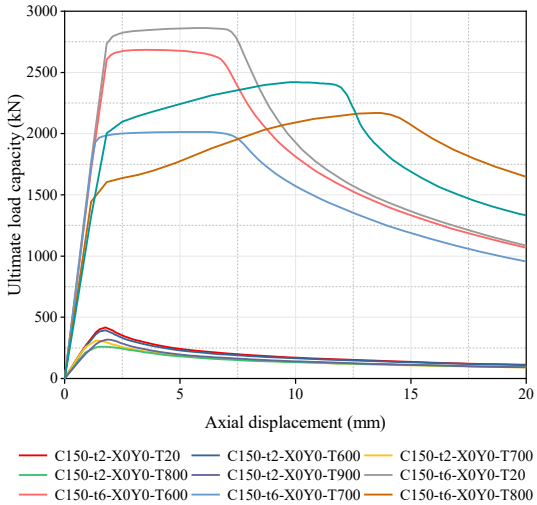

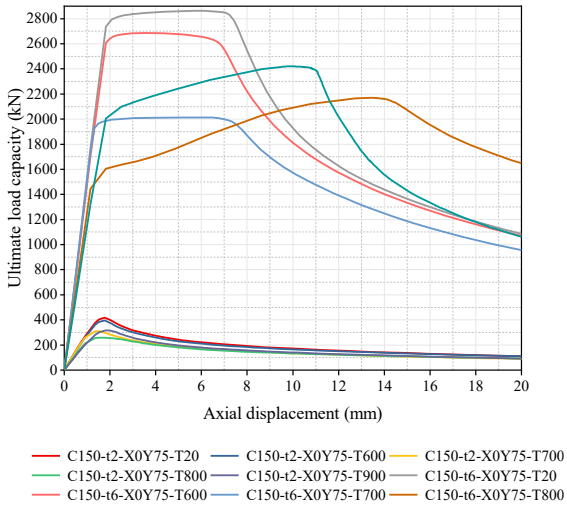

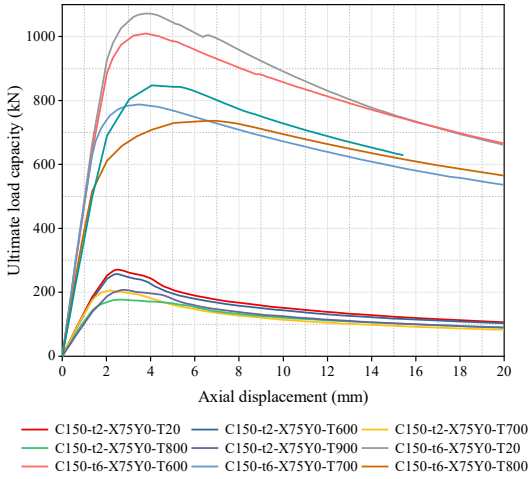
Ultimate load capacity (kN)
Axial displacement (mm)
C150-t2-X75Y0-T20
C150-t2-X75Y0-T600
C150-t2-X75Y0-T700
C150-t2-X75Y0-T800
C150-t2-X75Y0-T900
C150-t6-X75Y0-T20
C150-t6-X75Y0-T600
C150-t6-X75Y0-T700
C150-t6-X75Y0-T800

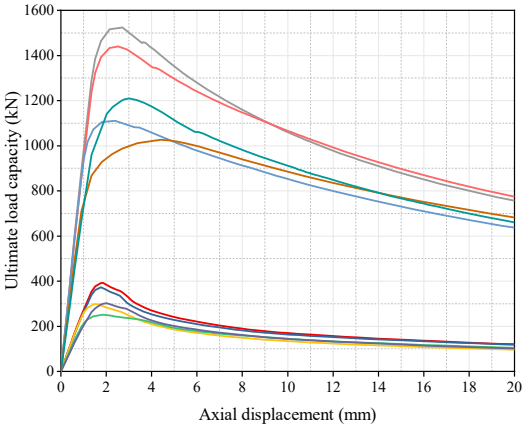
Ultimate load capacity (kN)
Axial displacement (mm)
C150-t2-X37.5Y37.5-T20
C150-t2-X37.5Y37.5-T600
C150-t2-X37.5Y37.5-T700
C150-t2-X37.5Y37.5-T800
C150-t2-X37.5Y37.5-T900
C150-t6-X37.5Y37.5-T20
C150-t6-X37.5Y37.5-T600
C150-t6-X37.5Y37.5-T700
C150-t6-X37.5Y37.5-T800

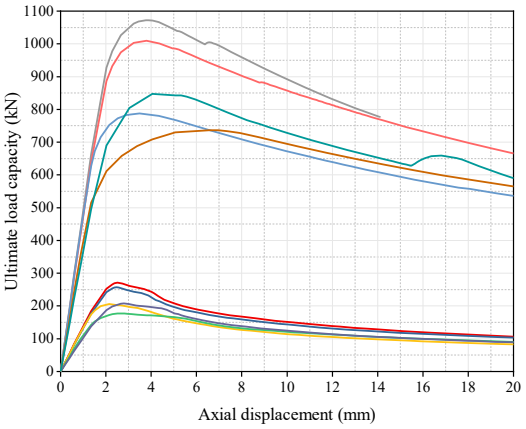
Ultimate load capacity (kN)
Axial displacement (mm)
C150-t2-X75Y75-T20
C150-t2-X75Y75-T600
C150-t2-X75Y75-T700
C150-t2-X75Y75-T800
C150-t2-X75Y75-T900
C150-t6-X75Y75-T20
C150-t6-X75Y75-T600
C150-t6-X75Y75-T700
C150-t6-X75Y75-T800

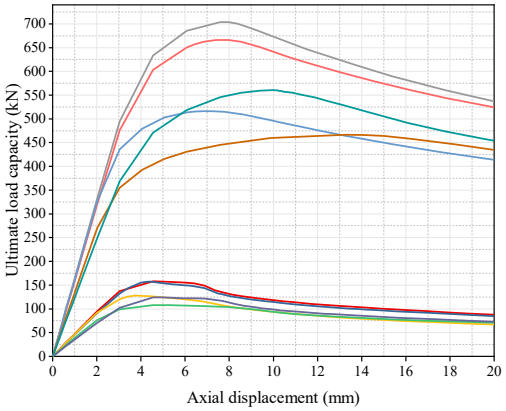
Ultimate load capacity (kN)
Axial displacement (mm)
C150-t2-X150Y150-T20
C150-t2-X150Y150-T600
C150-t2-X150Y150-T700
C150-t2-X150Y150-T800
C150-t2-X150Y150-T900
C150-t6-X150Y150-T20
C150-t6-X150Y150-T600
C150-t6-X150Y150-T700
C150-t6-X150Y150-T800

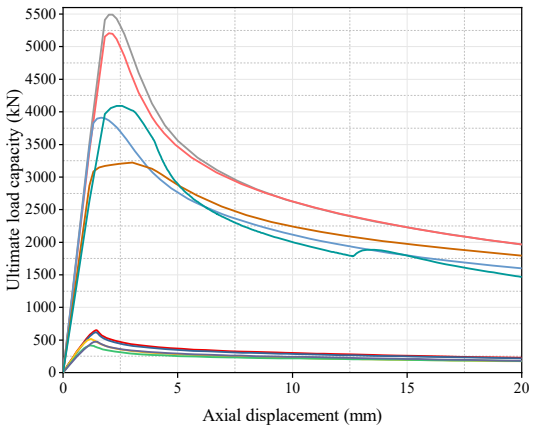
Ultimate load capacity (kN)
Axial displacement (mm)
C300-t2-X0Y0-T20
C300-t2-X0Y0-T600
C300-t2-X0Y0-T700
C300-t2-X0Y0-T800
C300-t2-X0Y0-T900
C300-t6-X0Y0-T20
C300-t6-X0Y0-T600
C300-t6-X0Y0-T700
C300-t6-X0Y0-T800

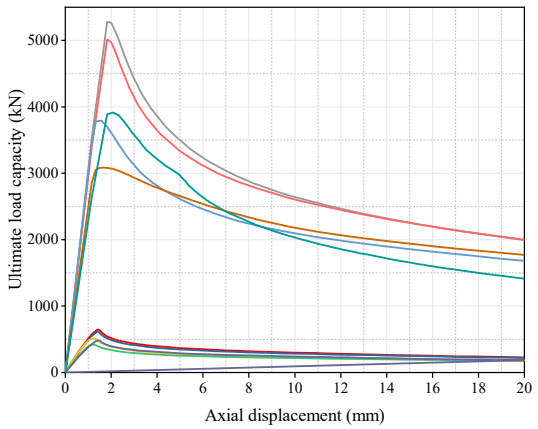
Ultimate load capacity (kN)
Axial displacement (mm)
C300-t2-X0Y75-T20
C300-t2-X0Y75-T600
C300-t2-X0Y75-T700
C300-t2-X0Y75-T800
C300-t2-X0Y75-T900
C300-t6-X0Y75-T20
C300-t6-X0Y75-T600
C300-t6-X0Y75-T700
C300-t6-X0Y75-T800

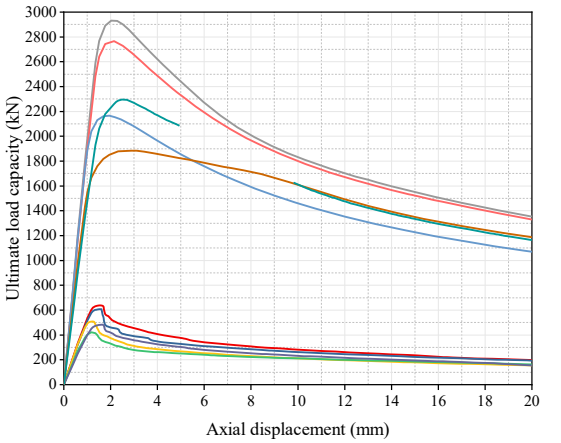
Ultimate load capacity (kN)
Axial displacement (mm)
C150-t2-X75Y0-T20
C150-t2-X75Y0-T600
C150-t2-X75Y0-T700
C150-t2-X75Y0-T800
C150-t2-X75Y0-T900
C150-t6-X75Y0-T20
C150-t6-X75Y0-T600
C150-t6-X75Y0-T700
C150-t6-X75Y0-T800

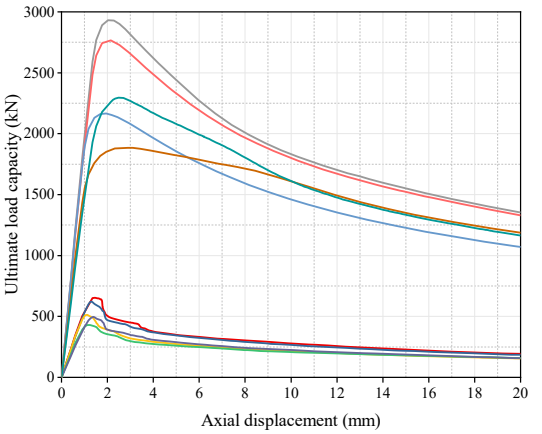
Ultimate load capacity (kN)
Axial displacement (mm)
C300-t2-X75Y75-T20
C300-t2-X75Y75-T600
C300-t2-X75Y75-T700
C300-t2-X75Y75-T800
C300-t2-X75Y75-T900
C300-t6-X75Y75-T20
C300-t6-X75Y75-T600
C300-t6-X75Y75-T700
C300-t6-X75Y75-T800

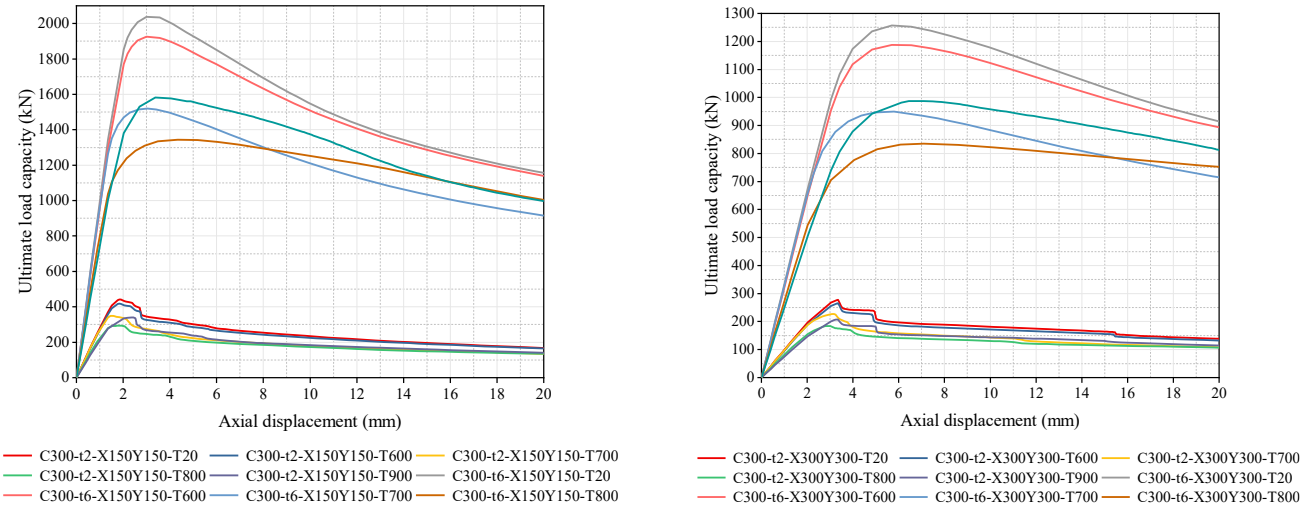

Fig. 8 Nonlinear analysis results for columns with circular cross-sectional shape.

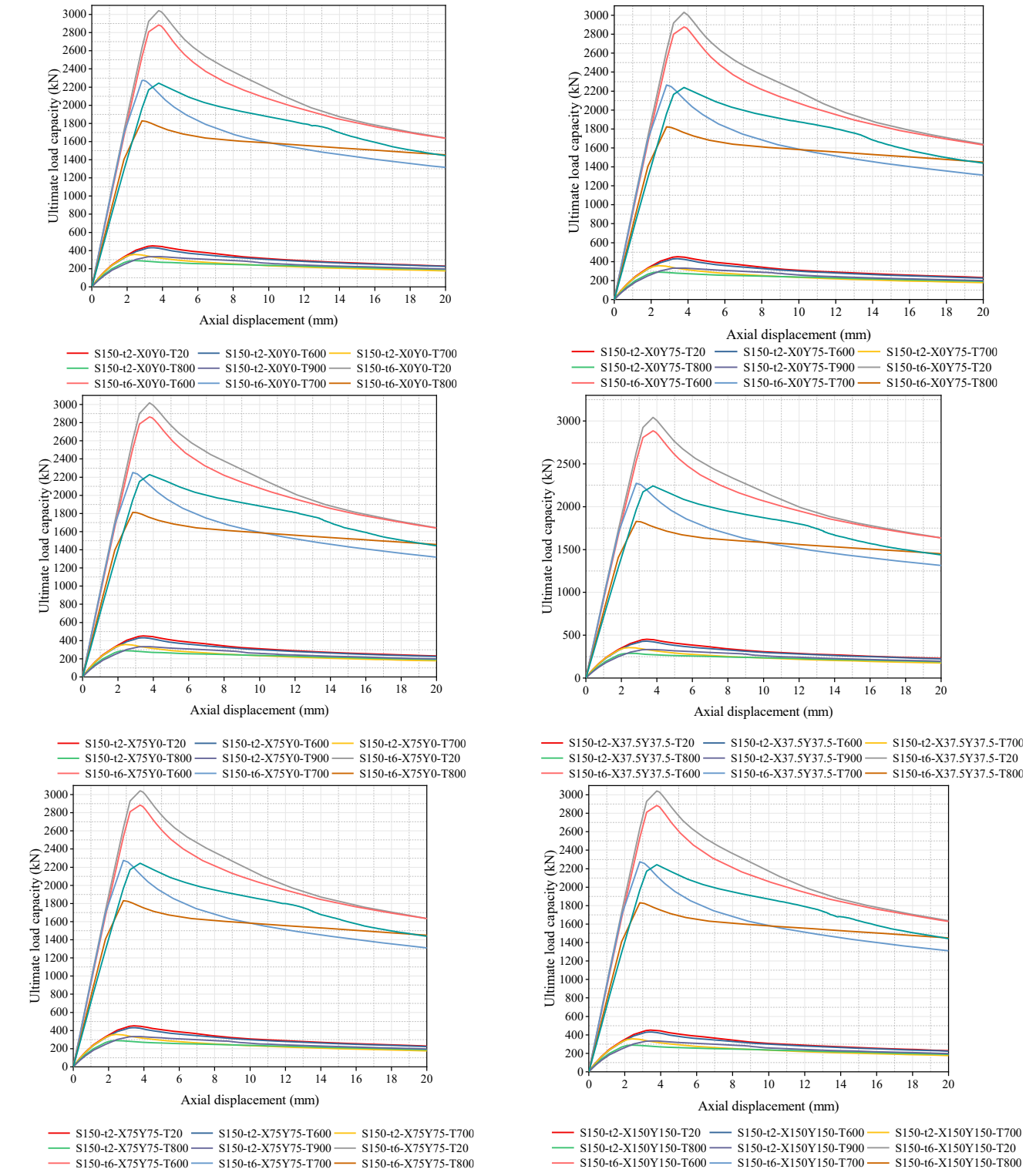

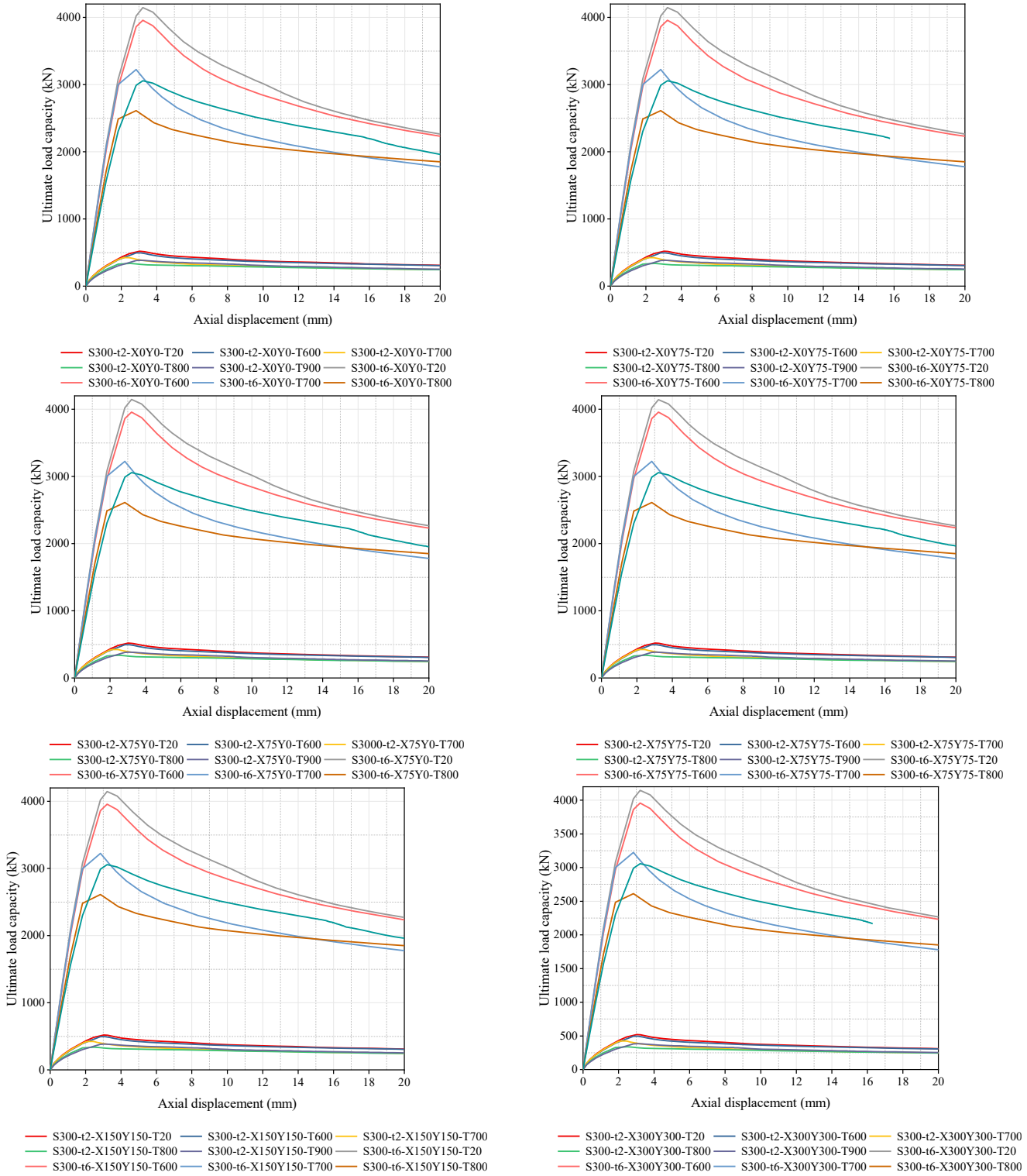

Fig. 9 Nonlinear analysis results for stub columns with a square cross-sectional shape.

4.1 Analyzing the Variables' Impact on the Ultimate Load Capacity of Stub Columns

Cross-sectional shape

The cross-sectional form of a column dramatically changes the structural performance of the column and the amount of load that the column can carry. This is particularly true in the case of fire and for the parameters of fire exposure temperature and eccentricity. The results presented here reveal that, in most cases, columns with circular cross-sections have a higher load capacity at the point of failure than square ones when subjected to the same loading and fire exposure conditions. In the schemes of the previous part, with a side length/diameter of 150 mm and a thickness of 2 mm (C150-t2 and S150-t2), the circular column had a higher load capacity at the point of failure than the square one. To be precise, when the scheme heated to 700°C was under investigation (C150-t2-X0Y0-T700 and S150-t2-X0Y0-T700), the circular column showed a load at failure that was about 10.5% higher than that of the square one. This means that columns with circular cross-sections perform better than those with square cross-sections at high temperatures. The difference becomes clearer at a high fire exposure temperature (e.g., 900°C as shown in C150-t2-X0Y0-T900 and S150-t2-X0Y0-T900), where the circular column had a load capacity at the point of failure that was 14.6% higher than that of the square one. The performance gaps between circular and square columns are owing to the shapes of their cross sections. A circular cross-section ensures that the material is more evenly distributed around the main axis, which is very important when the structure is subjected to axial compression in addition to higher eccentric loads. The sharp edges of a square column may lead to higher stress concentration in the edges when the structure is subjected to eccentric loads. A square column experiences a bigger drop in its structural efficiency at high temperatures than a circular cross-section of the same size. The geometric advantage of circular columns is shown by the regular and foreseeable increment of the ultimate load capacity with the time of exposure at high temperatures, including 600°C or 900°C, if it is assumed that the load capacity at the ultimate limit is reached. Eccentricities refer to the various geometrical changes of performance. Under eccentric load exposure at (X0Y75), circular columns displayed an average rise in ultimate load of 8.7% when compared to square columns subjected to the same eccentric and fire exposure conditions. As a result, the circular columns became less sensitive to the increase of eccentric conditions, and as the eccentricities

approached the mid-span moment, they still retained a comparatively higher load-carrying capacity. The impact of cross-sectional form on ultimate load capacity is revealed by Figure 10 for the cases of some columns at 900°C under real fire exposure; thus, the main emphasis is laid on the performance regarding ultimate load capacity.

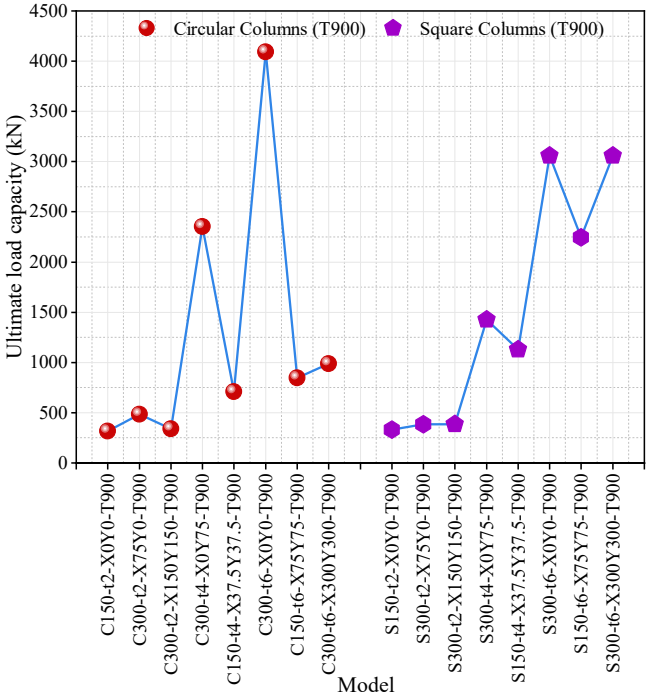

Fig. 10 Impact of cross-sectional shape on ultimate load capacity (900℃ exposure).

Dimension of cross-section

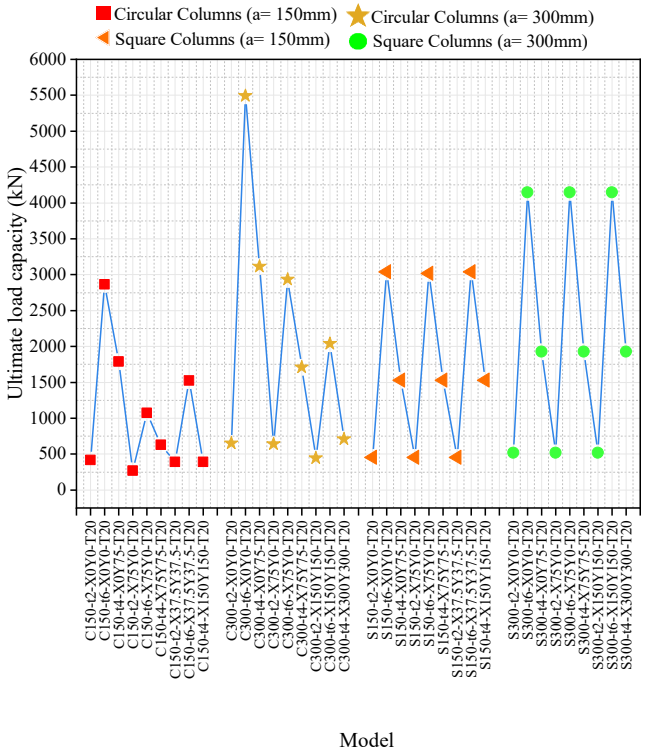

Figure 11 demonstrates the effect of the major dimension on the ultimate load capacity of round and square columns. The enhancement in ultimate load capacity by changing the primary dimension from 150 mm to 300 mm for both circular and square columns is quite notable. With a diameter of 300 mm, circular columns will show a considerable rise in load capacity as compared to 150 mm circular columns. Square columns show a rise in ultimate load capacity with a dimension of 300 mm; however, this increase is not as significant as that in circular columns. Circular columns are structurally more advantageous as they spread the material further from the axis, thereby resulting in better load resistance. The percentage differences of the ultimate load capacity, especially the disparity between the 150 mm and 300 mm cases, emphasize the effect of the primary dimension. The analysis of the relationship between the diameter of circular columns and ultimate load capacity reveals that a change from 150 mm to 300 mm results in a 30% rise in load capacity. The rise in the capacity of the square columns caused by the increase in side length is close to 25%. This emphasizes how important the cross-sectional area of the loaded columns is, especially those loaded eccentrically and exposed to fire. The plot's trends showed the percentage differences and confirmed the notable enhancement in load capacity of columns with larger major dimensions visually.

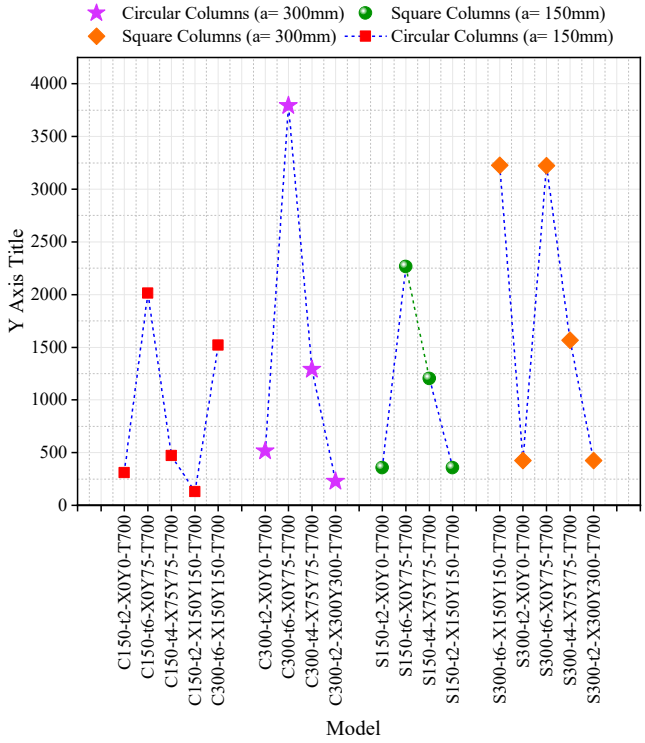

Fig. 11 Impact of cross-sectional dimension on ultimate load capacity.

Column's wall thickness

The analysis reveals that the ultimate load capacity has significantly improved as the wall thickness was elevated from 2mm to 4mm and from 4mm to 6mm. Both circular and square columns' ultimate load capacity follow a trend associated with an increase in wall thickness. As an example, the ultimate load capacity of columns having a 2mm wall thickness compared to columns with a 4mm wall thickness differs by about 30%. This means that just a slight increase in the thickness of the wall can improve the column's ability to carry the load in the case of a post-fire scenario and eccentric loading. The rise in the ultimate load capacity of the columns, in particular, the 4mm and 6mm ones, is quite significant regarding the percentage difference, which is about 20%. There is a direct relationship between the thickness of a column and its load-bearing capacity, which indicates that the thicker the wall, the better the overall performance will be. The wall thickness's impact on ultimate load capacity becomes even more notable when the fire is part of the scenario. At elevated temperatures (i.e., 600°C and 900°C), columns with thicker walls show better performance than those with thinner walls. The disparity in ultimate load capacity for the columns heated to 900°C and having a wall thickness of 2 mm and 6 mm, respectively, was around 40%; thus, the column with 6 mm thickness was able to resist thermal degradation and failure of material better and showed higher strength. The wall thickness considerably contributes to the fire resistance of the columns. The thickness of walls helps the column to keep its structural integrity under harsh thermal situations. The increased ultimate load capacity at very severe fire exposure conditions indicates that the wall thickness plays a decisive role in designing elements where fire safety is of primary concern. Figure 12 shows how wall thickness affects the ultimate load capacity in a post-fire situation. Each thickness (2 mm, 4 mm, and 6 mm) is represented as a separate point. This figure is a visual representation of the positive trend that the load-bearing capacity of thicker columns is higher after they have been subjected to fire. The outcomes of the test reveal that thick-walled columns were less affected by the respective factors causing elevated temperatures and degradation, and they also showed better performance regarding load capacity. The columns with thinner walls (2 mm) exhibited a very significant reduction in ultimate load capacities after being heated to high temperatures. Conversely, the load-bearing capacities of thick-walled columns are massively increased. Stability is very important in structures that have been or may be subjected to a long-lasting fire; thus, the safety of the structure depends on the columns being able to maintain their strength.

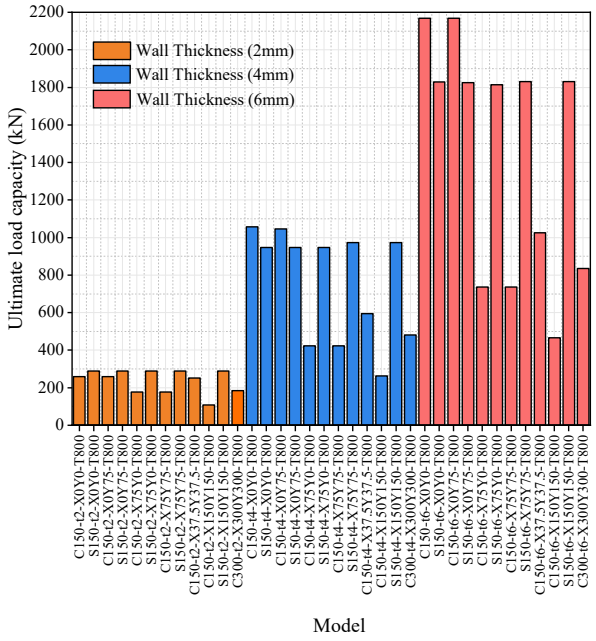

Fig. 12 Impact of wall thickness on ultimate load capacity (800℃ exposure).

Eccentricity

The research clearly shows that the ultimate load capacity of columns drops as eccentricity increases, and higher eccentricities cause the strongest reduction in this capacity. The columns that were tested at an eccentricity of 37.5 mm had a higher ultimate load capacity than the columns that were tested at 300 mm eccentricity. The 37.5 mm eccentricity led to a load capacity that was roughly 20% lower compared to the 75 mm case, thus confirming that a small increase in the eccentricity made a very significant difference in the load-carrying capacity of the columns. The comparison of the capacities of columns eccentrically loaded at 75 mm and 150 mm revealed that the load capacity was reduced by roughly 25%. That means the ultimate load capacity was very much compromised when the eccentricity was increased. The disparity in the reduction of the ultimate load capacity was at its maximum when the juxtaposition of the eccentricities of 150 mm and 300 mm was made. The percentage difference between the two setups was around 35%, and this is a clear symptom of a significant loss of load knowledge with increased eccentricity. The explicit variation of the ultimate load capacity with diverse eccentricities demonstrates the significance of the selection of appropriate eccentricities in column design because slight changes in eccentric loading can cause substantial changes in the ultimate load capacity.

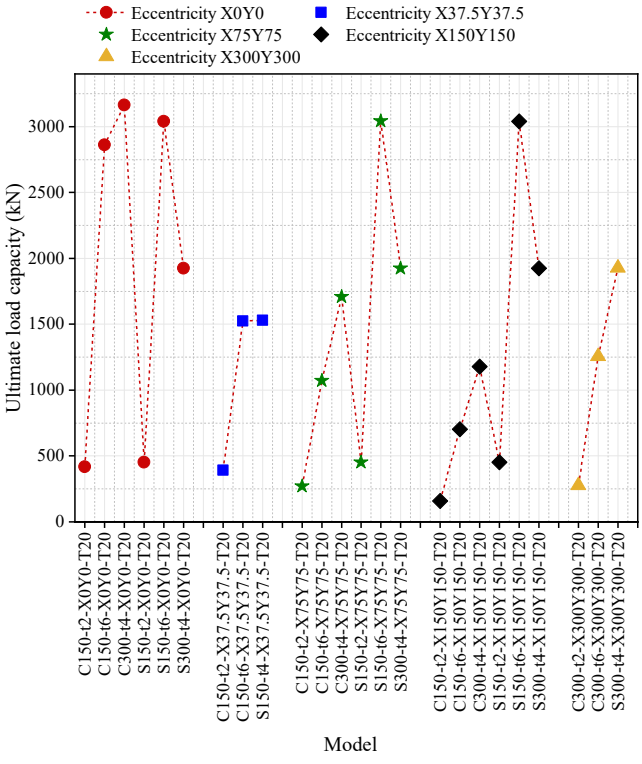

(a)

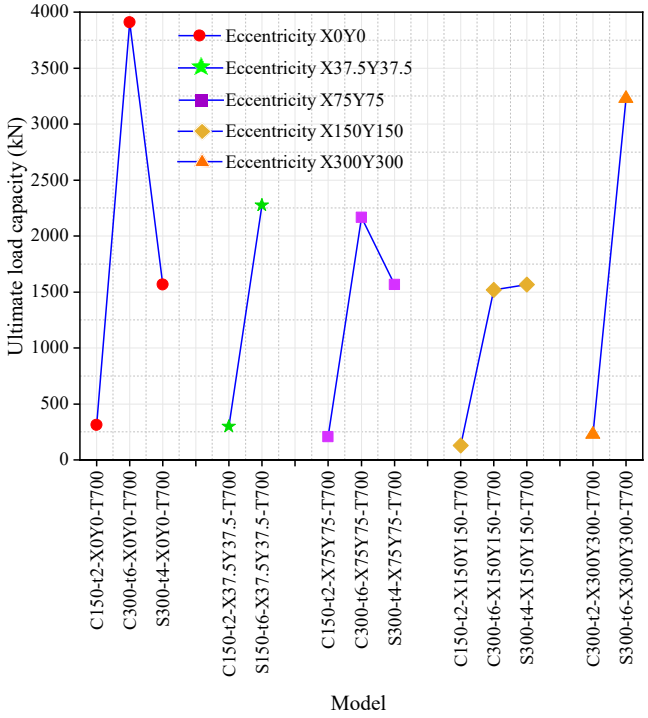

(b)

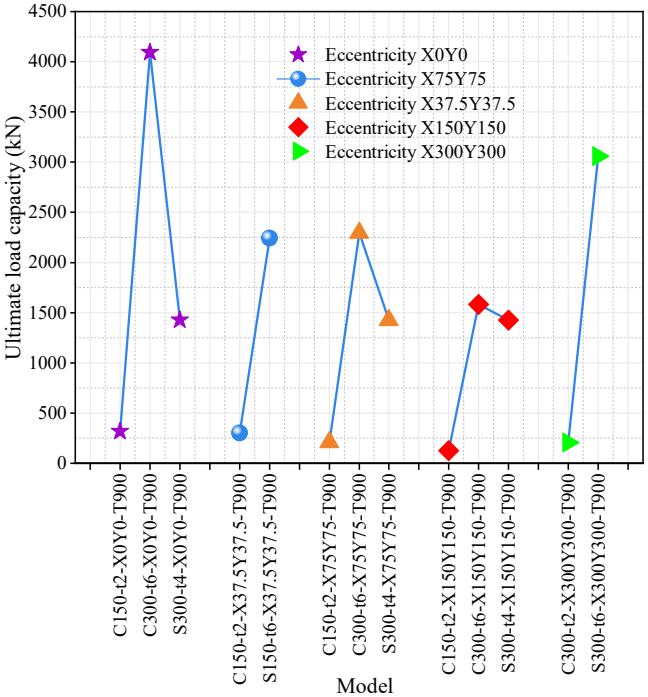

(c)

Fig. 13 Effect of eccentricity on ultimate load capacity, a) 20℃ exposures, b) 700℃ exposures, c) 900℃ exposures.

The findings presented in Figure 13 demonstrate that an increase in eccentricity in both the X and Y directions considerably decreases the column's capacity to support the ultimate loads.

4.2 Discussion on Failure Mode

The failure modes of cold-formed steel stub columns are influenced dramatically by several geometric and load-related factors, including the form of the cross-section, the thickness of the wall, the dimensions of the cross-section, and the eccentricity of the load. A consideration of these variables leads to specific structural consequences, which are the vital signs of the compressed column's stability. The impact of the cross-sectional form on the failure response has been explained with the help of Figure 14, which shows the profiles of the stub columns with the C-shaped and S-shaped cross-sections. The failure of the C-shaped columns was, in general, the local buckling of the web and flange areas; more specifically, these parts of the column got thinner due to the open and unbalanced configuration, which gave less resistance to the local instability. Conversely, the S-shaped columns - which have a more symmetric or closed configuration - were, to a great extent, a distortional buckling mode. This significant difference serves to underline that the geometric

symmetry and panel closure have an effect not only on the buckling behavior but also on the load-bearing capacity of the stub columns. Figure 15 compares the wall thickness of the columns regarding failure modes, thus showing the columns of 2mm, 4mm, and 6 mm thickness but with the same shape, section, and area. The thin-walled stub columns (t = 2 mm) were subjected to local and distortional buckling, resulting in the overall instability of the columns due to the authors' low morale and apprehensions regarding the capacity to resist instability. The stub columns with a 4 mm thick wall eventually bowed, demonstrating the transitional behavior through the combination of failure modes, local deformation, and flexural response. When the wall thickness was increased to t = 6 mm, local buckling was the major cause of failure; however, the failure mode changed to global buckling and some material crushing, thus showing that these types of columns reveal improved stability and strength. Figure 16 demonstrates how cross-sectional dimensions affect the changes in width and depth of the stub columns were studied while the wall thickness remained constant. At the smaller scale, buckling was very localized, and it was at the middle height or corners of the stub column that occurred most frequently. The deformation mode pointed to local instability as the most dominant form.

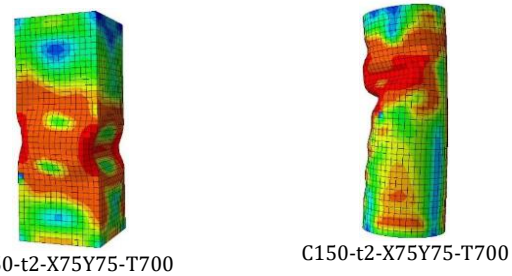

Fig. 14 Failure modes of stub columns with different cross-sectional shapes.

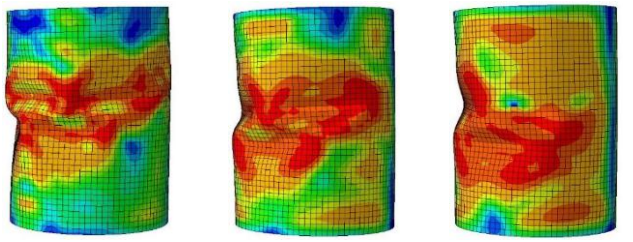

Fig. 15 Failure modes of stub columns with different wall thicknesses.

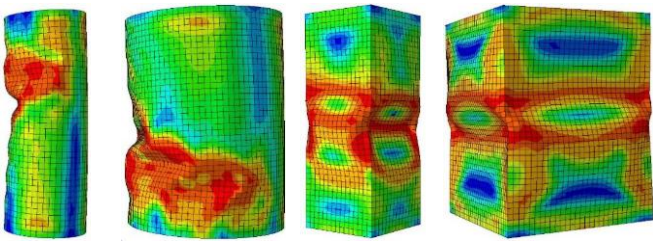

Fig. 16 Failure modes of stub columns with different dimensions of cross-sections.

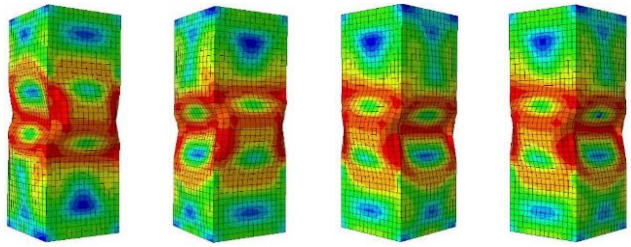

Fig. 17 Failure modes of stub columns with different loading eccentricities.

As the size was increased, the deformation patterns became more evenly spread, indicating a transition of failure modes from mainly local buckling to also include distortional and global buckling. The work points to the fact that with the bigger sections probably having a higher load capacity, they can also experience more complex interactions of the events and modes of buckling due to the increased slenderness and the interplay between local and global modes of buckling. The eccentricity of the load effect can be seen in Figure 17. In these columns, the eccentricity was in one of the two directions ('X' or 'Y') or they were under concentric loading (with zero eccentricity, 'X0Y0'). The concentrically loaded groups (X0Y0) were characterized by symmetric local buckling as well as a uniform stress distribution. The use of single directional eccentricity (X0Y75 or X75Y0) gave rise to asymmetric local buckling and deformations. The columns that had eccentricity in both directions (X75Y75 and X150Y150) appeared to have very pronounced asymmetric shapes, which, in the end, led to a combined axial-flexural failure because of early instability and the initial bending-dominated buckling mechanism inclination. The determinations are such that the increment of eccentricity leads to the ultimate capacity of stub columns being declined, as well as the failure mechanism being shifted completely. The eccentricity must be factored into the design process so that one can be safe from instability under actual loading conditions.

5. Conclusion

The exploration of the post-fire behavior of hollow section stub columns under eccentric axial compression thoroughly analyzes the subject by deeply examining the effect of the most important parameters: the shape of the cross-section, the axial dimensions, the thickness of the wall, and the value of the biaxial eccentricity. The research has developed and verified a numerical simulation of fire-damaged columns using experimental data; thus, the simulation reflects the complex interrelations between the geometrical and thermal parameters that determine the stability of fire-compromised columns in a very accurate way. As per the investigation, CHS columns retained more residual load capacity than square hollow section columns under both concentric and eccentric loading conditions, at least at high temperatures. The improved residual load capacity can be explained by the more uniform material distribution and lower stress concentration areas in circular columns. Moreover, the rise in cross-sectional area positively affects the ultimate load; the circular parts showed a more considerable increase in the ultimate load than the square ones, although they are of the same cross-sectional dimensions. The column thickness turned out to be the most significant factor for both the heat resistance and the mechanical performance of the column, since the higher thickness increased the available load-bearing capacity after the fire, implying that they can be used under fire conditions. The effect of the axial load eccentricity was also there, as larger eccentricities in either direction (X or Y) caused very considerable decreases in the residual capacity and changes of asymmetric deformation modes, including combination axial-flexural failures. The study explains the relationship between cross-sectional shape and wall thickness as factors influencing the transfer from local to global buckling and how structural failure processes become more abrupt and asymmetric as a result of increasing eccentricity. These findings underscore the significance of real geometric imperfections and actual loading when devising possible solutions in the field of fire-resistant design. The numerical database established in this study provides a valuable foundation for future development of design-oriented formulations. Although the present work primarily focuses on elucidating the post-fire mechanical behavior and governing parameters of hollow section stub columns, the identified trends in temperature, eccentricity, and geometry effects can serve as a basis for defining simplified reduction factors or modification coefficients for design codes, including Eurocode 3 and AISC.

References

Al-Thairy, H., & Al-Naqeeb, F. (2023). Numerical Investigation on the Behavior of Eccentrically Loaded LWRC Columns at Elevated Temperature. 4th International Conference on Architectural & Civil Engineering Sciences, 1-9. https://doi.org/10.24086/ICACE2022/paper.865

Azhari, F., Heidarpour, A., & Zhao, X. L. (2017). Post-fire behavior of cold-formed ultra-high strength steel tubular stub columns. In Tubular Structures XVI (pp. 305-310). CRC Press. https://doi.org/10.1201/9781351210843-37

Chen, J., Chan, T.-M., & Varma, A. H. (2020). Stub column behavior of cold-formed high-strength steel circular hollow sections under compression. Journal of Structural Engineering, 146(12), 04020277. https://doi.org/10.1061/(ASCE)ST.1943-541X.0002828

Chen, J., Fang, H., & Chan, T.-M. (2021). Design of fixed-ended octagonal shaped steel hollow sections in compression. Engineering Structures, 228, 111520. https://doi.org/10.1016/j.engstruct.2020.111520

Dadvand, A. (2025). Numerical Investigation of Sample Dimensions and Wall Geometry Effects on Slender Retaining Wall Behavior. Novel Approaches in Civil and Geotechnical Engineering, 1(01), 1-15.

Fang, H., Chan, T.-M., & Young, B. (2019). Behavior of octagonal high-strength steel tubular stub columns. Journal of Structural Engineering, 145(12), 04019150. https://doi.org/10.1061/(ASCE)ST.1943-541X.0002429

Golzadeh Ebrahimi, N. (2025). Investigation of the Behavior of Mechanically Deployed Anchors under Repeated Loading and Unloading. Novel Approaches in Civil and Geotechnical Engineering, 1(01), 38-51.

Grajçevci, F., Mujaj, A., Kryeziu, D., Rrudhani, G., & Shkodrani, N. (2024). Experimental and Numerical Research on the Behavior of Steel Columns with Circular Hollow Cross Sections. Civil Engineering Journal, 10(5), 1577-1588. https://doi.org/10.28991/CEJ-2024-010-05-014

He, A., Sun, Y., Wu, N., & Zhao, O. (2021). Testing, simulation and design of eccentrically loaded austenitic stainless steel CHS stub columns after exposure to elevated temperatures. Thin-Walled Structures, 164, 107885. https://doi.org/10.1016/j.tws.2021.107885

Hodovanets, E., & Kvocak, V. (2024). Analysis of Load Eccentricity in Cold-Formed Steel RHS Columns under Compression Considering Geometric Imperfections. Selected Scientific Papers-Journal of Civil Engineering, 19(1), 20240004. https://doi.org/10.2478/sspjce-2024-0004

Hu, J., & Li, W. (2022). Numerical Analysis on Post-Fire Resistance of High-Strength Circular CFST Stub Column in Axial Compression. Frontiers in Built Environment, 8, 883454. https://doi.org/10.3389/fbuil.2022.883454

Jandera, M., Gardner, L., & Machacek, J. (2008). Residual stresses in cold-rolled stainless steel hollow sections. Journal of Constructional Steel Research, 64(11), 1255-1263. https://doi.org/10.1016/j.jcsr.2008.07.022

Jinxue, H., & Xiaoyong, M. (2010). An experimental investigation on behavior of eccentric compression SRC columns after fire with heating-cooling effect. Journal of Suzhou University of Science and Technology: Engineering and Technology, 23(4), 21-25.

Khalaf, M. S., Ibrahim, A. M., Najm, H. M., Hassan, A., Sabri, M. M. S., Alamir, M. A., & Alarifi, I. M. (2022). Evaluation and prediction of the bending behavior of circular hollow steel tube sections using finite element analysis. Materials, 15(11), 3919. https://doi.org/10.3390/ma15113919

Li, D., Huang, Z., Uy, B., Thai, H.-T., & Hou, C. (2019). Slenderness limits for fabricated S960 ultra-high-strength steel and composite columns. Journal of Constructional Steel Research, 159, 109-121. https://doi.org/10.1016/j.jcsr.2019.04.025

Liu, J., Chan, T.-M., & Young, B. (2023). Cross-section behaviour of cold-formed high strength steel irregular hexagonal hollow section stub columns under combined compression and bending. Advances in Structural Engineering, 26(12), 2210-2227. https://doi.org/10.1177/13694332231157930

Liu, J.-Z., Ma, X., Gao, K., Chen, J., Li, S., & Guo, J. (2024). Local buckling behaviour of Q690 high strength steel press-braked elliptical hollow section stub columns: Testing, numerical modelling, and design. Thin-Walled Structures, 204, 112359. https://doi.org/10.1016/j.tws.2024.112359

Ma, J.-L., Chan, T.-M., & Young, B. (2015). Material properties and residual stresses of cold-formed high strength steel hollow sections. Journal of Constructional Steel Research, 109, 152-165. https://doi.org/10.1016/j.jcsr.2015.02.006

Mehari, Z. A., & Han, J. (2022). Investigations of the through-thickness residual stress distribution during the partial heating roll forming process of square and rectangular hollow steel sections. Engineering Reports, 4(11), e12515. https://doi.org/10.1002/eng2.12515

Meng, X., & Gardner, L. (2020a). Behavior and design of normal-and high-strength steel SHS and RHS columns. Journal of Structural Engineering, 146(11), 04020227. https://doi.org/10.1061/(ASCE)ST.1943-541X.0002728

Meng, X., & Gardner, L. (2020b). Testing of hot-finished high strength steel SHS and RHS under combined compression and bending. Thin-Walled Structures, 148, 106262. https://doi.org/10.1016/j.tws.2019.106262

Meng, X., & Gardner, L. (2021). Flexural buckling of normal and high strength steel CHS columns. Structures, 34, 4364-4375. https://doi.org/10.1016/j.istruc.2021.09.106

Qureshi, R., Van Coile, R., Hopkin, D., Gernay, T., & Khorasani, N. E. (2022). Reliability assessment of the US prescriptive standard for steel columns under fire. Structures, 40, 711-724. https://doi.org/10.1016/j.istruc.2022.04.049

Shi, Y., Wang, J., Zhou, X., Xue, X., & Li, Y. (2024). Post-fire mechanical properties of Q960 cold-formed thick-walled ultra-high-strength steel. Fire Technology, 60(3), 1917-1953. https://doi.org/10.1007/s10694-024-01555-3

Su, A., Jiang, K., Liang, Y., & Zhao, O. (2021). Post-fire behaviour and resistances of S690 high strength steel welded I-section stub columns. Thin-Walled Structures, 169, 108422. https://doi.org/10.1016/j.tws.2021.108422

Sun, Y., Wang, Z., Xia, J., Sarquis, F. R., & de Lima, L. R. O. (2024). Experimental and numerical study of aluminium alloy angle-section stub columns. Thin-Walled Structures, 205, 112361. https://doi.org/10.1016/j.tws.2024.112361

Sun, Z., & Su, A. (2025). Post-fire behaviour of Q960 ultra-high strength steel welded I-sections under major-axis combined loading. Thin-Walled Structures, 113795. https://doi.org/10.1016/j.tws.2025.113795

Systemes, D. (2021). Abaqus Product Documentation: Abaqus Analysis User's Manual. Version 2021. Dassault Systemes, Providence.

Uszball, S., & Knobloch, M. (2024). Post-fire structural material behaviour of high-and ultra-high-strength steels. https://doi.org/10.1002/stco.202500003

Wang, J., Afshan, S., Schillo, N., Theofanous, M., Feldmann, M., & Gardner, L. (2017). Material properties and compressive local buckling response of high strength steel square and rectangular hollow sections. Engineering Structures, 130, 297-315. https://doi.org/10.1016/j.engstruct.2016.10.023

Xing, Z., Jiang, M., San, B., Wang, J., & Wu, K. (2024). Fire behaviour of stainless steel circular hollow section stub columns: Experimental study and design. Thin-Walled Structures, 196, 111494. https://doi.org/10.1016/j.tws.2023.111494

Xing, Z., Wang, J., San, B., Jiang, M., & Wu, K. (2023). Cross-sectional behaviour of QN1803 high-strength stainless steel I-section stub columns in fire. Thin-Walled Structures, 193, 111282. https://doi.org/10.1016/j.tws.2023.111282

Zhang, J., Su, A., & Jiang, K. (2024a). Post-fire behavior and residual resistances of S890 ultra-high strength steel circular hollow sections under combined compression and bending. Engineering Structures, 316, 118519. https://doi.org/10.1016/j.engstruct.2024.118519

Zhang, J., Su, A., & Jiang, K. (2024b). Post-fire behavior and residual resistances of S890 ultra-high strength steel circular hollow sections under combined compression and bending. Engineering Structures, 316, 118519. https://doi.org/10.1016/j.engstruct.2024.118519

Zhang, J., Su, A., Yang, H., Zhao, J., & Wang, Y. (2024c). Experimental and numerical investigations of S890 and S960 ultra-high strength steel circular hollow section columns. Engineering Structures, 311, 118143. https://doi.org/10.1016/j.engstruct.2024.118143

Zhang, J., Yang, H., & Su, A. (2024a). Post-fire behavior and resistances of S890 ultra-high strength steel circular hollow section beam-columns. Thin-Walled Structures, 204, 112322. https://doi.org/10.1016/j.tws.2024.112322

Zhang, J., Yang, H., & Su, A. (2024b). Post-fire behavior and resistances of S890 ultra-high strength steel circular hollow section beam-columns. Thin-Walled Structures, 204, 112322. https://doi.org/10.1016/j.tws.2024.112322

Zhang, J., Yang, H., Su, A., & Jiang, K. (2025). Experimental and numerical investigations of S890 and S960 ultra-high strength steel circular hollow section stub columns after fire exposure. Thin-Walled Structures, 209, 112933. https://doi.org/10.1016/j.tws.2025.112933

Zhao, H., Wang, Z., Zhang, W., Wang, R., Yang, D., & Lam, D. (2024). Performance of round-ended recycled aggregate CFST stub columns after fire exposure. Journal of Constructional Steel Research, 212, 108311. https://doi.org/10.1016/j.jcsr.2023.108311

Zhong, Y., Sun, Y., Tan, K. H., & Zhao, O. (2021). Post-fire behaviour and residual resistances of S700 high strength steel tubular section stub columns under combined loading. Thin-Walled Structures, 169, 108275. https://doi.org/10.1016/j.tws.2021.108275

Zhong, Y., Sun, Y., Zhao, O., & Gardner, L. (2022). Structural response and residual capacity of S700 high-strength steel CHS columns after exposure to elevated temperatures. Journal of Structural Engineering, 148(6), 04022050. https://doi.org/10.1061/(ASCE)ST.1943-541X.0003341

Zhong, Y., Tan, K. H., & Zhao, O. (2021). Experimental and numerical investigations of S700 high strength steel tubular section stub columns after exposure to elevated temperatures. Thin-Walled Structures, 163, 107669. https://doi.org/10.1016/j.tws.2021.107669

Zhou, F., Huang, L., & Li, H.-T. (2022). Cold-formed stainless steel SHS and RHS columns subjected to local-flexural interactive buckling. Journal of Constructional Steel Research, 188, 106999. https://doi.org/10.1016/j.jcsr.2021.106999

Zhou, H., Wang, W., Wang, K., & Xu, L. (2019). Mechanical properties deteriorate high strength steels after high temperature exposure. Construction and Building Materials, 199, 664-675. https://doi.org/10.1016/j.conbuildmat.2018.12.058

Zuo, W., Chen, M.-T., & Young, B. (2024). Structural behaviour of cold-formed steel elliptical hollow section stub columns after exposure to ISO-834 fire curve. Thin-Walled Structures, 197, 111309. https://doi.org/10.1016/j.tws.2023.111309

Disclaimer